 CMES, vol.7, no.3, pp.293-304, 2005

Finite Element Analysis of Carbon Nanotubes with Stone-Wales Defects

L. Nasdala[1], G. Ernst[1], M. Lengnick[1] and H. Rothert[1]

Abstract: Like any other geometric structure or building, carbon nanotubes may break down due to either material failure or structural failure. In this paper, it is shown that the failure mechanism of carbon nanotubes not only depends on the type and direction of loading but also on the location and number of defects. For the finite element simulations we use a new 4-node finite element without rotational degrees of freedom based on the force field method. For the examples shown here, mainly a single-walled (10,10) armchair nanotube with different Stone-Wales defects, the material parameters are directly taken from the DREIDING force field.

For carbon nanotubes subject to tension a kind of material failure, i. e. a breaking of bonds, can be observed. For carbon nanotubes subject to bending, an interesting question is whether they fail due to a breaking of bonds in the tension zone, which would be similar to the tension experiment, or due to a snap-through of bonds in the compression zone. From our FE simulations, it can be concluded that neither of these two failure mechanisms, but local buckling in the compression zone can be observed. From a mechanical point of view, however, it is not a pure bifurcation problem because the buckles are formed relatively slowly which corresponds more to a snap-through problem. For carbon nanotubes subject to torsion, we have to distinguish between bifurcation problems which are the case for defect-free nanotubes and snap-through problems which can be observed for those with defects. In all cases the Stone-Wales defects are responsible for a reduction of the maximum load, about 10 % for tension and bending, and up to 30 % for torsion.

keyword: Carbon nanotubes, Stone-Wales defects, DREIDING force field, finite element method, four-node element

[1] University of Hannover, Germany

1 Introduction

From a continuum-mechanical point of view, a prediction of material behavior is based on the assumption that the systems under consideration include enough particles allowing for averaging processes. As a result, numerous experimental observations like damping behavior cannot be readily explained. Thus, there is a considerable effort to find descriptions for strength and failure properties of materials, taking into account their atomic structure, see e. g. [Ghoniem and Cho (2002)].

Finite element methods proved themselves for decades as a high-performance procedure especially for the simulation of physical processes in the framework of continuum mechanics. Nevertheless, this method can also be applied efficiently to atomistic processes if adequate elements were formulated taking into account the discrete structure of systems. Force fields provide a solid basis for the development of such elements which describe the atomic interactions like bond stretching, bond bending and bond torsion with general force constants and geometric parameters.

To reduce numerical costs, often only a small part of a structure is simulated using molecular dynamics while other parts are assumed to be homogeneous so that continuum mechanics is applied. This leads to multiscale simulations coupling molecular dynamics (MD) and continuum mechanics. Shen and Atluri (2005) propose the use of meshless local Petrov-Galerkin (MLPG) methods [see also Atluri (2004)] to derive stiffness matrices as a link between continuum and MD calculations. Another possibility is the use of a lattice statics-based tangent-stiffness method proposed by Chung, Namburu, and Henz (2003). The advantage of the present FE approach for the atomic simulation via finite elements instead of the classical MD method is that it combines atomic and continuum simulation in one method. Using these approaches, the behavior of several types of nanostructures can be predicted. For an overview of the various applications and potentials in nanotechnology the

reader is referred to the papers by Brenner, Shenderova, Areshkin, Schall, and Frankland (2002), Srivastava and Atluri (2002) and Srivastava, Menon, and Cho (2001).

Topological defects – in particular adjacent pentagon/heptagon pairs, called Stone-Wales defects – have been proposed to play a major role in the growth and subsequent annealing down to the structurally ordered ground state of carbon nanostructures. They consist of a C-C bond rotated by an angle of 90 degrees, creating two pentagons and heptagons. Once formed, the pentagons/hexagons could move along the structure, creating either dislocation centers in regions of positive (pentagons) or negative (heptagons) Gaussian curvature, which ultimately lead to the closing of the nanostructure, see Miyamoto, Rubio, Berber, Yoon, and Tománek (2004). Moreover, Stone-Wales defects appear at the core of many relevant structural transformations governing, for example, the coalescences of nanotubes, the formation of pure intramolecular junctions for isoelectronic devices, and the onset of either plastic or brittle response of nanotubes subject to mechanical strain. Furthermore, the study of defect formation is motivated by the importance of their role in the electron transport properties of carbon nanotubes, see Buongiorno Nardelli, Yakobson, and Bernholc (1998b). The Stone-Wales defects also have a strong influence on large-scale structural rearrangements in graphite networks [Yoon, Han, Kim, Lee, Berber, Osawa, Ihm, Terrones, Banhart, Charlier, Grobert, Terrones, Ajayan, and Tománek (2004)].

Wei, Cho, and Srivastava (2003) found that the yielding or failure of carbon nanotubes is mainly dependent on the activation and propagation of defects, such as Stone-Wales bond rotation or graphitic sp^2 to sp^3 diamond-like bonding transitions at the location of collapse. The former has been mainly formed on tensile strained carbon nanotubes, whereas the latter has been mainly observed on axially compressed tubes. Theoretical and numerical simulation studies have shown that, under large tensile strain, Stone-Wales bond rotations result in the formation of pentagon-heptagon pair 5-7-7-5 defects on the nanotubes, which are energetically favorable at tensile strain larger than 5 %. Zhang, Lammert, and Crespi (1998) found that under an external force above the plastic threshold, proliferation of bond rotation defects is eventually halted by a repulsive defect-defect interaction.

Goal of this paper is to investigate the failure mechanism of carbon nanotubes with different kinds of Stone-Wales defects when subject to tension, bending and torsion. For our finite element simulations we use a new 4-node finite element based on the force field method which is introduced in the following section.

2 Formulation of a force field based finite element method

2.1 DREIDING force field

The potential energy of molecular systems like carbon nanotubes can be calculated with the force field method. A common approach for the calculation of carbon nanotubes is the use of the Tersoff-Brenner potential, see e. g. Yang, Han, Anantram, and Jaffe (2002) and Wei, Srivastava, and Cho (2002). We apply the DREIDING approach which is described by Mayo, Olafson, and Goddard (III) (1990), among others. Neglecting inversion and non-bonded interactions, the potential energy of this generic force field is of the form

$$E = E_{\mathrm{B}} + E_{\mathrm{A}} + E_{\mathrm{T}} \quad . \tag{1}$$

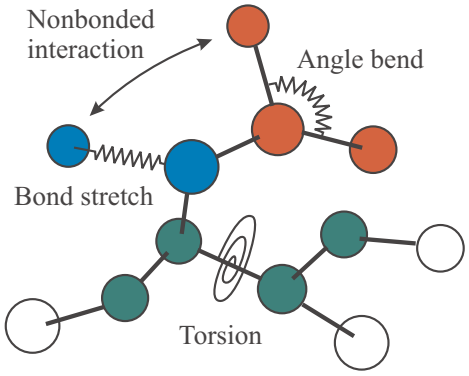

Figure 1 : Atomic interactions according to force field method

The different kinds of atomic interactions are shown in Fig. 1. The bond between two atoms I and J can be described by the Morse function [Morse (1929)]

$$E_{\mathrm{B}} = D_{\mathrm{e}} \left[\exp(-\beta \tilde{R}_{IJ}) - 1\right]^2 \tag{2}$$

with $\tilde{R}_{IJ} := R_{IJ} - R_{\mathrm{e}}$ and $\beta := \alpha n$.

The first and second derivatives of Eq. 2 with respect to R_{IJ} lead to the corresponding spring force

$$F_{\mathrm{B}} = -2\beta D_{\mathrm{e}} \left[\exp(-2\beta \tilde{R}_{IJ}) - \exp(-\beta \tilde{R}_{IJ})\right] \tag{3}$$

and the nonlinear spring constant

$$c_{\mathrm{B}} = 4\beta^2 D_{\mathrm{e}} \left[\exp(-2\beta\tilde{R}_{IJ}) - \frac{1}{2}\exp(-\beta\tilde{R}_{IJ}) \right] \quad , \qquad (4)$$

respectively. Fig. 2 shows the bond stretching energy E_{B} (Eq. 2), the bond stretching force F_{B} (Eq. 3) and the bond stretching spring constant c_{B} (Eq. 4) for an interatomic range $1\,\text{Å} \leq R_{IJ} \leq 2\,\text{Å}$.

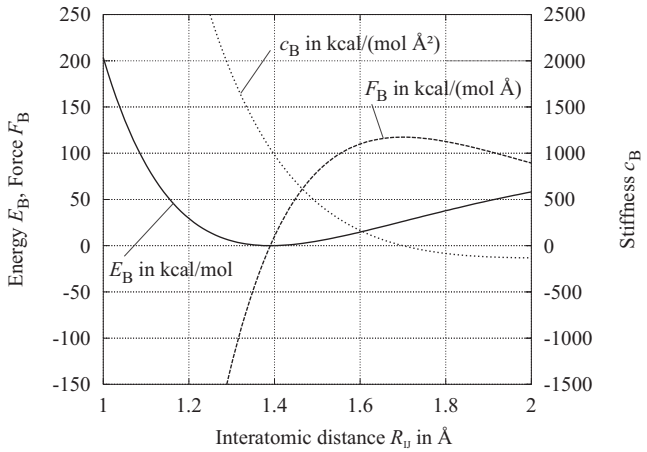

Figure 2 : Bond stretching energy E_{B}, bond stretching force F_{B} and bond stretching spring constant c_{B} according to DREIDING force field

The C-C bond length of graphite is 1.42 Å [Desch (1934)]. In the case of carbon nanotubes, the C-C bond length is known to be slightly larger than graphite: 1.44 Å [Saito, Dresselhaus, and Dresselhaus (1998)]. The increase of bond length reveals that even undeformed carbon nanotubes contain potential energy. According to Mayo, Olafson, and Goddard (III) (1990), the distance between two carbon atoms I and J is $R_{\mathrm{e}} = 1.39\,\text{Å}$ at the equilibrium state. For carbon, the bond order is $n = 1.5$. Further, $\alpha = 1.491\frac{1}{\text{Å}}$ and $D_{\mathrm{e}} = 105\frac{\text{kcal}}{\text{mol}}$.

For two bonds IJ and JK sharing a common atom, the three-body angle bend terms are of the harmonic cosine form

$$E_{\mathrm{A}} = \frac{1}{2} C_{IJK} \left[\cos\Theta_{IJK} - \cos\Theta_J^0 \right]^2 \qquad (5)$$

where Θ_{IJK} is the angle between bonds IJ and JK and C_{IJK} is the corresponding bending stiffness, see Fig. 3. The equilibrium angle Θ_J^0 is assumed to be independent of I and K, see Mayo, Olafson, and Goddard (III) (1990).

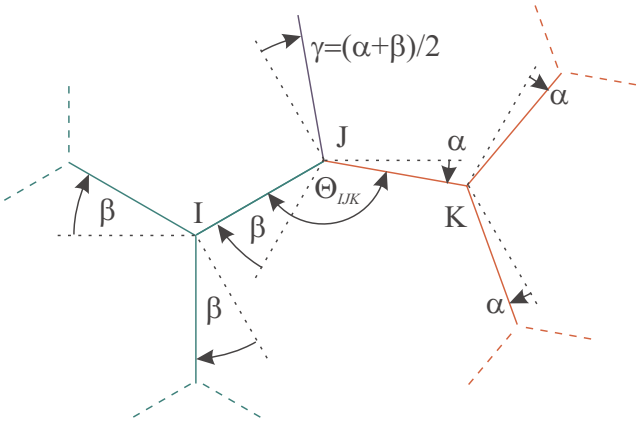

Figure 3 : Change of bond angle Θ_{IJK} illustrated by means of a planar deformation of a graphite layer

Derivation of Eq. 5 with respect to Θ_{IJK} yields the bending moment

$$M_{\mathrm{A}} = -C_{IJK} \left[\cos\Theta_{IJK} - \cos\Theta_J^0 \right] \sin\Theta_{IJK} \quad . \qquad (6)$$

The second derivative of Eq. 5 with respect to Θ_{IJK} results into the nonlinear spring constant

$$c_{\mathrm{A}} = C_{IJK} [\cos\Theta_J^0 \cos\Theta_{IJK} - \cos(2\Theta_{IJK})] \quad . \qquad (7)$$

Fig. 4 shows the bond bending energy E_{A} (Eq. 5), the bond bending moment M_{A} (Eq. 6) and the nonlinear bond bending spring constant c_{A} (Eq. 7) for $\Theta_J^0 = 120°$ and $C_{IJK} = 133.3\frac{\text{kcal}}{\text{mol rad}^2}$.

The torsion interaction for two bonds IJ and KL connected via a common bond JK is of the form

$$E_{\mathrm{T}} = \frac{1}{2} V_{JK} \left[1 - \cos\left[n_{JK} (\varphi_{IJKL} - \varphi_{JK}^0) \right] \right] \qquad (8)$$

where φ_{IJKL} is the dihedral angle (angle between the IJK and JKL planes), n_{JK} is the periodicity (an integer), V_{JK} is the barrier to rotation (always positive), and φ_{JK}^0 is the equilibrium angle, see Mayo, Olafson, and Goddard (III) (1990).

The first derivative of Eq. 8 with respect to φ_{IJKL} yields the torsional moment

$$M_{\mathrm{T}} = \frac{1}{2} V_{JK}\, n_{JK} \sin\left[n_{JK} (\varphi_{IJKL} - \varphi_{JK}^0) \right] \quad . \qquad (9)$$

Finally, the second derivative of Eq. 8 with respect to φ_{IJKL} results into the nonlinear torsion spring constant

$$c_{\mathrm{T}} = \frac{1}{2} V_{JK}\, n_{JK}^2 \cos\left[n_{JK} (\varphi_{IJKL} - \varphi_{JK}^0) \right] \quad . \qquad (10)$$

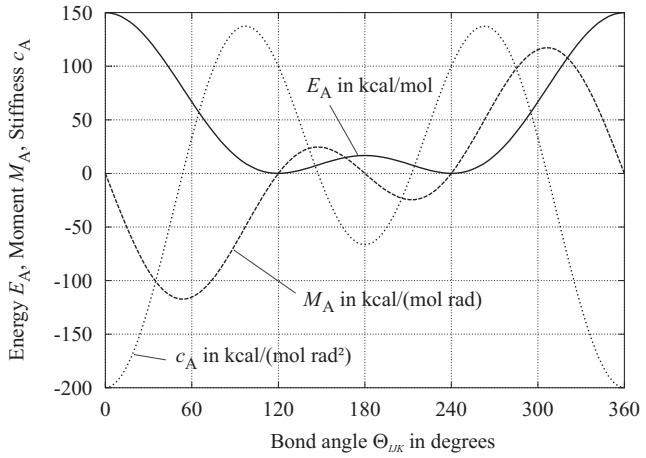

Figure 4 : Bond bending energy E_A, bond bending moment M_A and bond bending spring constant c_A according to DREIDING force field

Fig. 5 shows the bond torsion energy E_T (Eq. 8), the bond torsion moment M_T (Eq. 9) and the nonlinear bond torsion spring constant c_T (Eq. 10) for $\varphi^0_{JK} = 0°$ and 180°, $n_{JK} = 2$ and $V_{JK} = 25 \frac{\text{kcal}}{\text{mol rad}^2}$.

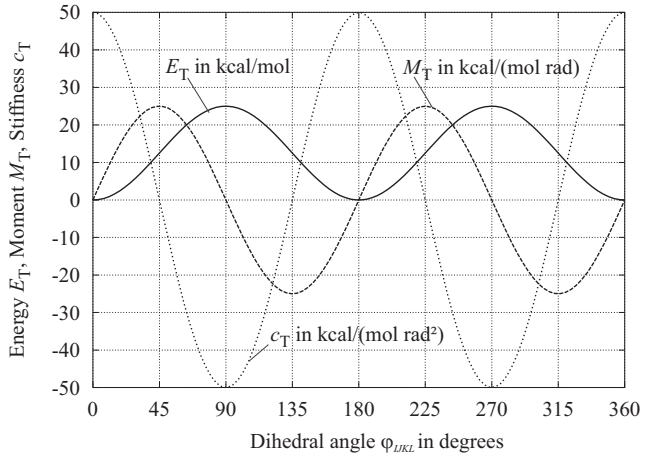

Figure 5 : Bond torsion energy E_T, bond torsion moment M_T and bond torsion spring constant c_T according to DREIDING force field

The force field method provides a suitable interface between physically accurate quantum-mechanical approaches, on the one hand, and numerically efficient continuum-mechanical approaches, on the other hand. Force fields adequately describe the real physics of nanostructures which makes them attractive as a tool to analyze material properties like damping behavior, fatigue cracking or fracture behavior. In addition, force fields provide an excellent theoretical basis for the application of the finite element method due to the analogy to multi-body systems with atoms as mass points and the different kinds of bonds as spring elements. Finite element programs offer comprehensive pre- and postprocessing tools as well as sophisticated solvers which allow for the modelling, calculation and visualization of complex structures.

2.2 The new 4-node finite element

A simulation of the mechanical behavior of nanostructures using finite elements with rotational degrees of freedom, i. e. beam or shell elements, results in fundamental difficulties. As shown by Nasdala and Ernst (accepted), the parameter identification is ambiguous and the rotational degrees of freedom lead to incorrect deformations.

An atom as a point object has no rotational degrees of freedom which must be taken into account by an appropriate finite element model. This section contains a brief description of a new 4-node finite element shown in Fig. 6 which overcomes the disadvantages of beam and shell elements because it uses only translational degrees of freedom.

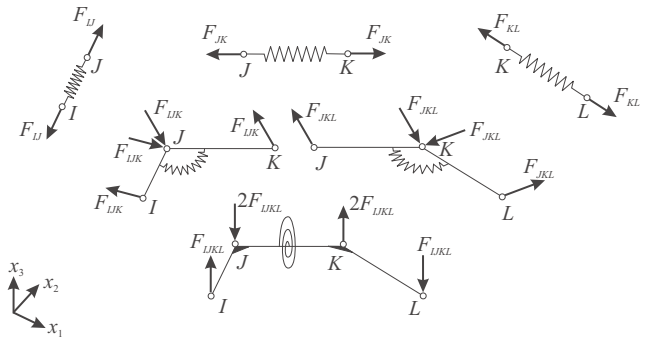

Figure 6 : Four-node finite element consisting of three tension, two bending and one torsion subelements

The new element has four nodes with the position vectors $\mathbf{x}_I$, $\mathbf{x}_J$, $\mathbf{x}_K$ and $\mathbf{x}_L$ as primary unknowns. For the bond between the two atoms I and J the DREIDING force field described in section 2.1 yields the bond stretching force

$$F_{IJ} = -2\beta \frac{D_e}{12} \left[\exp(-2\beta \tilde{R}_{IJ}) - \exp(-\beta \tilde{d}_{IJ}) \right] \qquad (11)$$

with $\tilde{R}_{IJ} = |\mathbf{x}_I - \mathbf{x}_J| - R_e$. Similar expressions can be derived for the bonds between the two atoms J and K and K and L, respectively:

$$\begin{aligned} F_{JK} &= -2\beta\frac{D_e}{12}\left[\exp(-2\beta\tilde{R}_{JK}) - \exp(-\beta\tilde{R}_{JK})\right] \\ F_{KL} &= -2\beta\frac{D_e}{12}\left[\exp(-2\beta\tilde{R}_{KL}) - \exp(-\beta\tilde{R}_{KL})\right] \quad . \end{aligned} \tag{12}$$

For two bonds IJ (JK) and JK (KL) sharing a common atom, the three-body angle bend terms corresponding to Eq. 6 are

$$\begin{aligned} F_{IJK} &= -\frac{C_{IJK}}{4R_e}\left[\cos\Theta_{IJK} - \cos\Theta_J^0\right]\sin\Theta_{IJK} \\ F_{JKL} &= -\frac{C_{JKL}}{4R_e}\left[\cos\Theta_{JKL} - \cos\Theta_K^0\right]\sin\Theta_{JKL} \quad . \end{aligned} \tag{13}$$

According to Eq. 9 the torsion interaction for two bonds IJ and KL connected via a common bond JK yields the moment

$$F_{IJKL} = \frac{V_{JK}}{4\sqrt{3}R_e}\, n_{JK} \sin\left[n_{JK}(\varphi_{IJKL} - \varphi_{JK}^0)\right] \quad . \tag{14}$$

The bending angles $\Theta_{IJK} = \Theta_{IJK}(\mathbf{x}_I, \mathbf{x}_J, \mathbf{x}_K)$ and $\Theta_{JKL} = \Theta_{JKL}(\mathbf{x}_J, \mathbf{x}_K, \mathbf{x}_L)$ as well as the torsion angle $\varphi_{IJKL} = \varphi_{IJKL}(\mathbf{x}_I, \mathbf{x}_J, \mathbf{x}_K, \mathbf{x}_L)$ depend on the coordinates $\mathbf{x}_I$, $\mathbf{x}_J$, $\mathbf{x}_K$ and $\mathbf{x}_L$.

Each carbon atom is neighbored by three other carbon atoms. Thus when superposing all four-node elements, this results in twelve normal spring subelements being placed between the atoms J and K, four bending subelements between three atoms I, J and K and four torsional spring subelements between two atoms J and K. For this reason, Eq. 3, Eq. 6 and Eq. 9 are premultiplied by the factors $1/12$, $1/4$ and $1/4$, respectively, which leads to Eqs. 11 to 14. Furthermore, Eqs. 13 and 14 take into account the lever arms R_e and $\sqrt{3}R_e/2$ of the bending and torsional moments. The element formulation takes into account finite deformations which allows for simulating fracture processes in carbon nanotubes.

Assembling the nodal forces to the global residuum vector $\mathbf{R}$ leads to a system of nonlinear equations

$$\mathbf{R}(\mathbf{x}) = \mathbf{0} \tag{15}$$

with $\mathbf{x}$ as global position vector of the current coordinates. The solution of these equations is achieved using a Newton-Raphson iterative procedure:

$$\mathbf{K}(\mathbf{x}_k)\cdot\mathbf{u} = -\mathbf{R}(\mathbf{x}_k) \quad . \tag{16}$$

The stiffness matrix $\mathbf{K}$ is the derivative of the residual forces with respect to the coordinates

$$K_{ij}(\mathbf{x}_k) = \left.\frac{\partial R_i}{\partial x_j}\right|_{\mathbf{x}_k} \quad , \tag{17}$$

see [Nasdala and Ernst (accepted)] for details. The subscripts i and j denote the degree of freedom whereas the subscript k denotes the iteration step. The constitutive equations are linearized in a consistent form which yields a quadratic convergence of the Newton-Raphson solution procedure. The displacement increment $\mathbf{u}$ has to be added to the coordinates

$$\mathbf{x}_{k+1} = \mathbf{x}_k + \mathbf{u} \tag{18}$$

until the displacement increment or rather the residual vector $\mathbf{R}$ are sufficiently small. If all forces are in equilibrium the right hand side vector is zero.

Compared to a standard beam approach, the developed four-node element has the advantage that only translational degrees of freedom are used in the formulation. This corresponds to a basic assumption made in standard molecular dynamics simulations where molecules or atoms are defined as a system of interacting material points, whose motion is described dynamically with a vector of instantaneous positions and velocities. Furthermore, the new element is computationally efficient because it has only three degrees of freedom per node instead of six of a beam element.

An additional advantage of the new four-node element compared with a standard beam element is that no parameter identification procedure is required. The parameters can be taken directly from the equations defining the force field.

The vectors of the carbon atoms defining their initial positions (i. e. positions of the atoms before an external load is applied) only have to be given approximatively. This configuration, which in general is a non-equilibrium one, can be equilibrated during a (numerically damped) relaxation step. There is no need to introduce initial strains or stresses because the equilibrium distance R_e between two atoms as well as the equilibrium angles Θ_j^0 for the three-body angle bend terms and the equilibrium angle φ_{JK}^0 for the torsion interaction for two bonds IJ and KL connected via a common bond JK are intrinsic parts of this finite element.

Furthermore the use of subelements allows for a decoupling of the potential energies E_B, E_A and E_T, in contrast to a pure beam approach where the material parameters (in particular the torsional rigidity and out of plane bending stiffness) are ambiguous since torsion energy is caused by bending as well as by torsion.

3 Failure mechanisms in carbon nanotubes

3.1 Perfect carbon nanotubes under uniaxial tension

In this subsection we compare the results obtained with the new four-node finite element for two types of nanotubes under axial loading with results published by Zhou and Shi (2001). Molecular dynamics (MD) simulations have been performed by the authors to study the mechanical properties of two types of single-walled carbon nanotubes under tensile loading with and without hydrogen storage. Brenner's bond order hydrocarbon potential was used in their simulations, see Mowrey, Brenner, Dunlap, Mintmire, and White (1991) and Dunlap, Brenner, and Schriver (1994).

The examined nanotubes, a $(10,10)$ armchair and a $(17,0)$ zigzag type, have a similar diameter and tube length. A periodic boundary condition has been used by Zhou and Shi along the axial and horizontal directions. To simulate the tubes under tensile loading, the tubes were annealed at simulation temperature for 5000 MD increments during the first simulation step. The time interval between two MD increments was chosen to 0.5 fs. In the second simulation step the tubes were pulled incrementally in axial direction with a strain increment of 5×10^{-4}. Following each increment of pulling, some additional MD increment were used to relax the structure [Zhou and Shi (2001)].

Fig. 7 and Fig. 8 show the calculated load-deflection curves for the perfect (17,0) zigzag and (10,10) armchair carbon nanotubes, respectively. Because single-walled carbon nanotubes are constructed of hexagonal carbon rings, their mechanical properties are strongly dependent on their chiral directions. Bond angle and bond length are the two crucial factors that control the deformation. Though length and diameter of both nanotubes are almost identical, see Tab. 1, only the initial stiffnesses (i. e. the slope of the load-deflection curve for zero strain) of the different nanotube types are similar: $S_0 \approx 1016\,\text{nN}$ for the (17,0) zigzag nanotube and $S_0 \approx 1047\,\text{nN}$ for the (10,10) armchair nanotube. The maximum force of

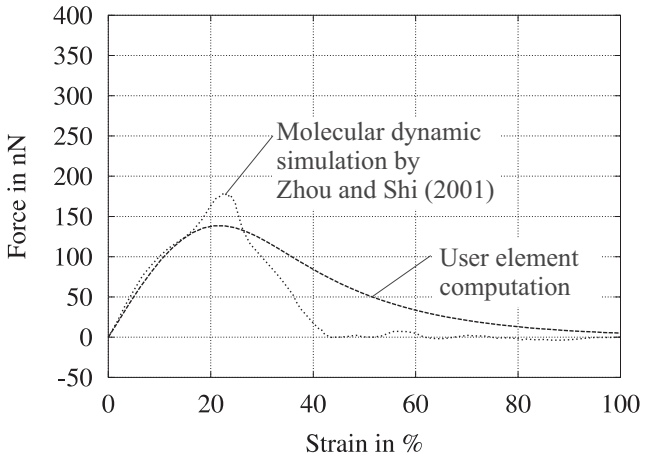

Figure 7 : Load-deflection curves for a (17,0) zigzag carbon nanotube subject to uniaxial tension. The results obtained by Zhou and Shi (2001) using molecular dynamics simulation and the results obtained by the authors with the new four-node finite element are shown.

the (10,10) armchair nanotube, $F_{max} \approx 175.2\,\text{nN}$, however, and the corresponding elongation, $\varepsilon_{max} \approx 28.0\,\%$, are much higher than the maximum force of the (17,0) zigzag nanotube, $F_{max} \approx 138.4\,\text{nN}$, and the corresponding elongation $\varepsilon_{max} \approx 20.7\,\%$, respectively. Here, we define the maximum elongation ε_{max} and the maximum tensile force F_{max} at the turning point on the load-deflection curve that has the highest value of F.

Table 1 : Structural parameters of the carbon nanotubes

Type of nanotube	(17,0)	(10,10)
diameter in Å	13.47	13.72
length in Å	71.59	71.02
number of atoms	1190	1200
mass of a carbon atom in fg	1.994473×10^{-8}	

A detailed examination of the nanotube structure during the deformation process by Zhou and Shi (2001) revealed that the elongation of the (10,10) nanotube is initially due to the altering of bond angles (stage 1). For armchair single-walled carbon nanotubes, the elongation of tube due to the altering of bond angles can be up to 15 % if the C-C bonds are assumed to be rigid. For zigzag single-walled carbon nanotubes one-third of the C-C bonds are

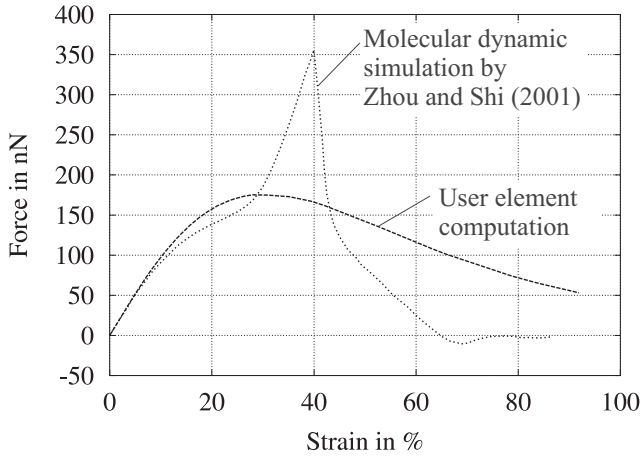

Figure 8 : Load-deflection curves for a (10,10) armchair carbon nanotube subject to uniaxial tension. The results obtained by Zhou and Shi (2001) using molecular dynamics simulation and the results obtained by the authors with the new four-node finite element are shown.

parallel to the loading axis and the loading force is then directly acting on these bonds. Under further pulling, the contribution from the elongation of the C-C bonds becomes significant and plays the main role in the deformation process (stage 2). When the strain is up to a critical level, some groups of the C-C bonds are broken. Then, the tube starts necking and the force decreases dramatically. Due to the nature of the hexagonal carbon ring, pulling the zigzag tube along its axial direction would cause some second nearest neighbor C-C atoms to become closer and to form new C-C bonds. In the local regions of these newly formed bonds, some old carbon-carbon bonds have to break due to the saturation of covalent bonds. This would lead to the necking and breakage of the zigzag single-walled carbon nanotubes (stage 3).

The results obtained during stages 1 and 2 with the two different methods (molecular dynamic approach and finite element method) are in good agreement, see Figs. 7 and 8. At the limit point, the maximum interatomic distance in axial direction is $R_{IJ} \approx 1.700\,\text{Å}$. For larger distances, $R_{IJ} > 1.700\,\text{Å}$, the normal stiffness c_B (Eq. 4) becomes negative, see Fig. 2, which can be interpreted as a kind of softening. In the mathematical sense, a bifurcation problem occurs at this deformation state of the carbon nanotube. The fact that the static analysis remains on the instable primary path can be attributed to the perfect symmetry of the carbon nanotubes. This stability problem for geometrically perfect nanotubes under uniaxial displacement-driven loading is assumed to be one of the reasons for the differences between the two load-deflection curves obtained with molecular dynamics simulations and finite element method, respectively.

3.2 Carbon nanotubes with Stone-Wales defects

Atomistic studies have suggested that carbon nanotubes possess unique and superior electrical, electromechanical, and mechanical properties, and therefore have many potential applications in the fields of nanoelectronics, nanoelectro-mechanical systems (NEMS) and nanocomposites. However, there are some discrepancies between atomistic modelling and experimental results. For example, Yakobson, Campbell, Brabec, and Bernholc (1997) molecular dynamics simulations based on the empirical interatomic potential for carbon suggested that the breaking strain of a single wall CNT is as large as 55 %, while the fracture strain of multiwall carbon nanotubes measured by Yu, Lourie, Dyer, Moloni, Kelly, and Ruoff (2000) is less than 12 %. One important reason for this large difference is that most atomistic studies have not accounted for the effect of defects in carbon nanotubes. Belytschko, Xiao, and Ruoff (2002) showed that defects can explain part of the discrepancy between the failure stresses and strains of nanotubes given by theoretical or numerical predictions and those observed in experiments.

In the following the influence of Stone-Wales defects on the mechanical behavior of a (10,10) armchair carbon nanotube with structural parameters given in Tab. 1) are studied. The orientation of the defects and their distribution over the nanotube is thought to have a significant influence on the mechanical, electrical and thermal behavior of the nanostructure. Therefore, we introduced a defect distribution function which specifies all defects in the nanotube by their lattice indices. For real-world simulations, this function should be specified on the basis of experiments and an accompanying statistical investigation. Here, we restrict our calculations to systems with a maximum of two Stone-Wales defects equally distributed along the axis of the nanotube or in circumferential direction.

Fig. 9 shows the different defect distributions (locations and orientations of the Stone-Wales defects) taken into account. The defects are grouped into

- defect group 0, no defect,

- defect group 1, one Stone-Wales defect at location $(n_{d_{11}}, m_{d_{11}}) = (12,0)$,
- defect group 2, two Stone-Wales defects at locations $(n_{d_{21}}, m_{d_{21}}) = (8,0)$ and $(n_{d_{22}}, m_{d_{22}}) = (16,0)$,
- defect group 3, two Stone-Wales defects at locations $(n_{d_{31}}, m_{d_{31}}) = (8,0)$ and $(n_{d_{32}}, m_{d_{32}}) = (8,8)$.

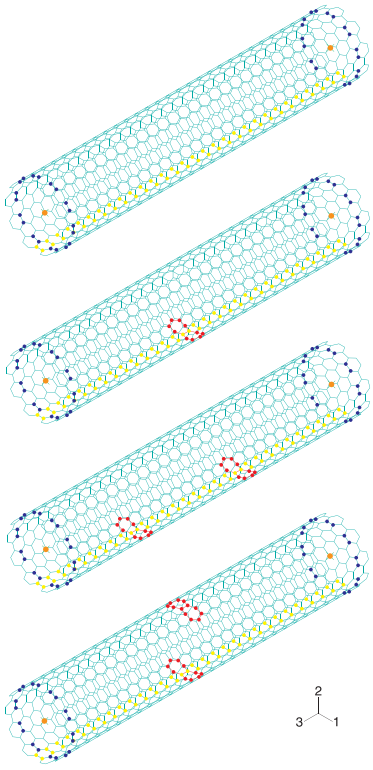

Figure 9 : (10,10) armchair carbon nanotubes; top down: no defect (dg0), one Stone-Wales defect at the bottom (dg1), two Stone-Wales defects at the bottom (dg2), two Stone-Wales defect with one at the top and one at the bottom (dg3)

In contrast to a static analysis, in a dynamic analysis it is not possible to increase the deflection linearly with time because inertial forces would become infinite. For that reason the loading velocity is increased with time, slowly enough to get a quasi-static response. The load is prescribed at the two ends of the tube where the marked nodes are rigidly connected to each other.

3.2.1 Tension test

Fig. 10 shows the load-deflection curve of a (10,10) armchair carbon nanotube in the uniaxial tension mode for different defect groups 0, 1, 2 and 3 computed with the new four-node finite element. We can observe that the carbon nanotube with defects collapse earlier than the perfect nanotube.

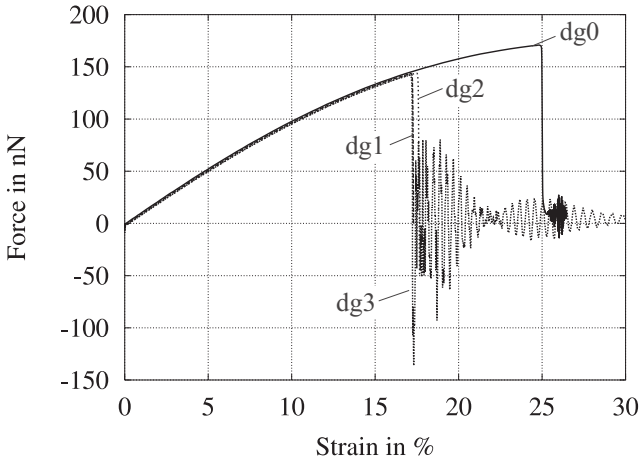

Figure 10 : Load-deflection curves for the (10,10) armchair carbon nanotubes subject to tension

In Fig. 11 the configurations of the (10,10) carbon nanotube with defect groups 1, 2 and 3 at ultimate loading are shown. One can observe the localization of deformations in the vicinity of the Stone-Wales defects in all the three cases. In these localization zones the distances between neighboring atoms are so large that the normal stiffness of the four-node element becomes negative. This behavior introduces a kind of local softening in the defective atomic areas finally resulting in the breaking and reorientation of interatomic bonds.

Fig. 10 shows that the ultimate load is almost independent of the number and locations of the Stone-Wales defects as long as at least there is one defect. For all defect groups we have computed an ultimate load of about 150 nN and a corresponding strain of about 17 %. Of course this result refers to the nanotubes and the defect distributions examined here and cannot be generalized without further research. Particularly the initial defect distributions must be adapted to actual data by the evaluation of tests. Furthermore, it has to be observed that in strained nanotubes at high temperatures the spontaneous formation of double pentagon-heptagon defect pairs oc-

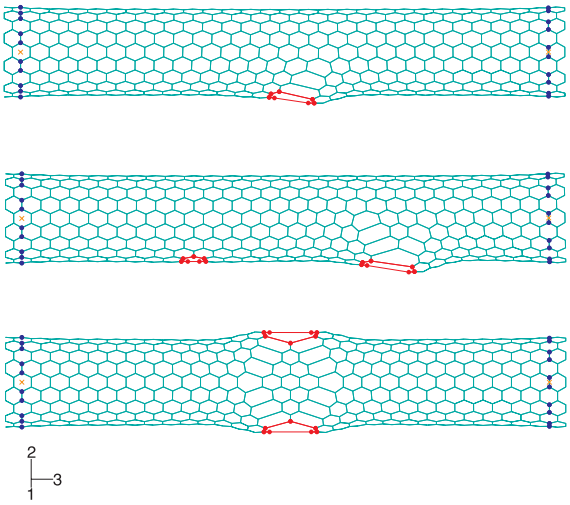

Figure 11 : Deformed configuration of the (10,10) armchair carbon nanotubes at about 17 % uniaxial strain

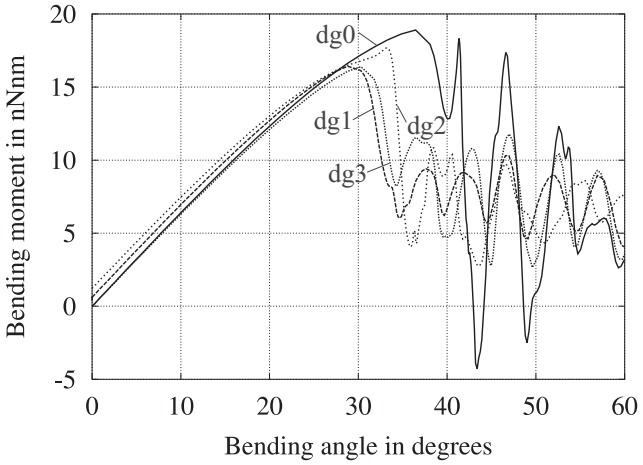

Figure 12 : Load-deflection curves for the (10,10) armchair carbon nanotubes subject to bending

curs. Tubes containing these defects are energetically preferred to uniformly stretched tubes at strains greater than 5 %, see Buongiorno Nardelli, Yakobson, and Bernholc (1998b,a). These topological defects act as nucleation centers for the formation of dislocations in the originally ideal graphite network, and they constitute the onset of a plastic deformation of the carbon nanotube. The mechanism of formation of such defects, their energetics, and transformations are not included in the theoretical framework used here for studying the tensile instabilities of the (10,10) armchair carbon nanotube.

3.2.2 Bending test

Fig. 12 shows the behavior of the nanotubes when subject to bending. In this case, the influence of the Stone-Wales defects on the global mechanical behavior of the carbon nanotube is not as obvious as in the uniaxial tension case. The defects are acting as geometrical imperfections transforming the bifurcation problem to a snap-through problem. For more information about stability problems the interested reader is referred to [Crisfield (1996, 1997)]. The ultimate bending moment for the perfect (10,10) carbon nanotube was calculated to about 19 nNnm, appearing at a bending angle of about 37 degrees. A single defect (defect group 1) reduces the ultimate bending moment by about 10 % to the value of 17 nNnm. It is interesting to observe that the second initial defect in the (10,10) carbon nanotube does not lead to a further reduction of the ultimate bending moment, see Fig. 12. Nevertheless, the difference between to two curves obtained for defect groups 2 and 3 indicate that the location of the defects has a significant influence on the global mechanical behavior in the bending mode and should be taken into account at the calculation of limit loads.

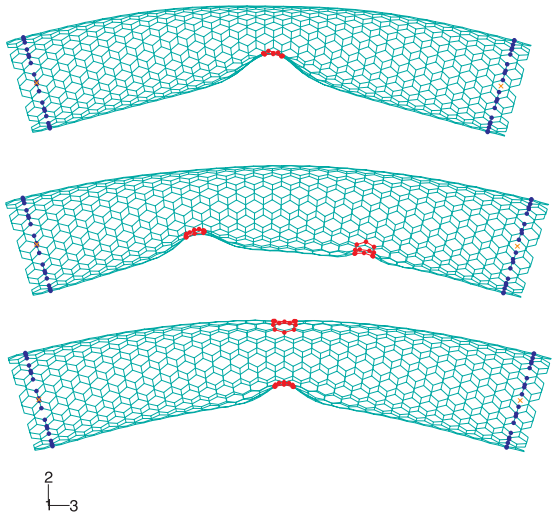

Figure 13 : Deformed configuration of the (10,10) armchair carbon nanotubes at bending angle of about 32 degrees

In Fig. 13 the configurations at ultimate bending moments are shown. Compared with the configurations be-

longing to uniaxial tension, the initial Stone-Wales defects are not connected with the occurrence of localized deformations under large strains in the defective areas. Nevertheless, large curvatures of the lattice can be observed in the surrounding of the defects which lie in the compression zone requiring a suitable choice of the bending and torsion terms of the underlying potential. Unlike this, the initial curvatures of the lattice in the vicinity of defects located in the tension zone is flattened out by the overlayed bending mode.

3.2.3 *Torsion test*

Fig. 14 shows the load deflection curve of the nanotubes when subject to torsion. In this case the ultimate torsion moment is strongly influenced by the Stone-Wales defects. The perfect carbon nanotube passes a bifurcation point at a torsion moment of about 26 nNnm, however due to the geometric imperfections introduced by the Stone-Wales defects the defective tubes show a snap-through behavior. Under the given conditions, the influence of the number and orientations of defects on the ultimate torsion moment is rather low. Its value ranges from about 16 nNnm for the nanotube with defect group 1 to about 15 nNnm for the nanotube with defect group 3. Nevertheless, the occurrence of a single defect reduces the ultimate torsion moment by about 40 % from about 26 nNnm to about 16 nNnm.

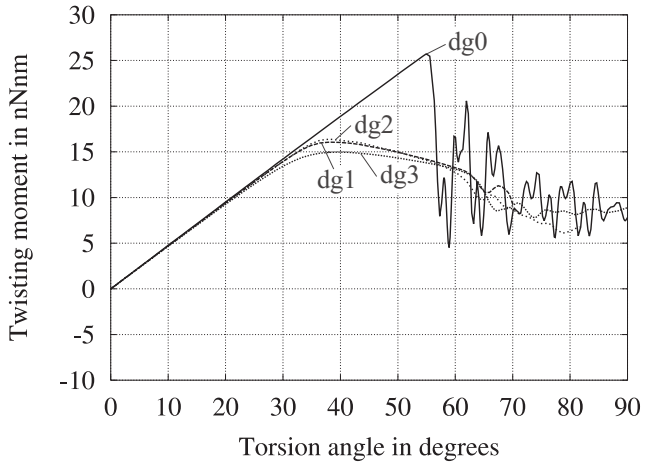

Figure 14 : Load-deflection curves for the (10,10) armchair carbon nanotubes subject to torsion

In Fig. 15 the nanotubes during collapse are shown. The ultimate torsion angle for all three configurations is about 40 degrees. As in the bending case the initial Stone-Wales defects do not lead to a local failure in the defective areas due to tearing of bonds. Also, the large curvatures of the lattice in the surrounding of the defects observed in the bending mode are not present in this deformation mode. Nevertheless, a comparison of the results presented in Figures Fig. 12 and Fig. 14 shows that the ultimate torsion moment is much more reduced by the occurrence of a single defect than the ultimate bending moment. Certainly, this result should not be generalized because it depends strongly on the chirality of the nanotubes and the type of loading.

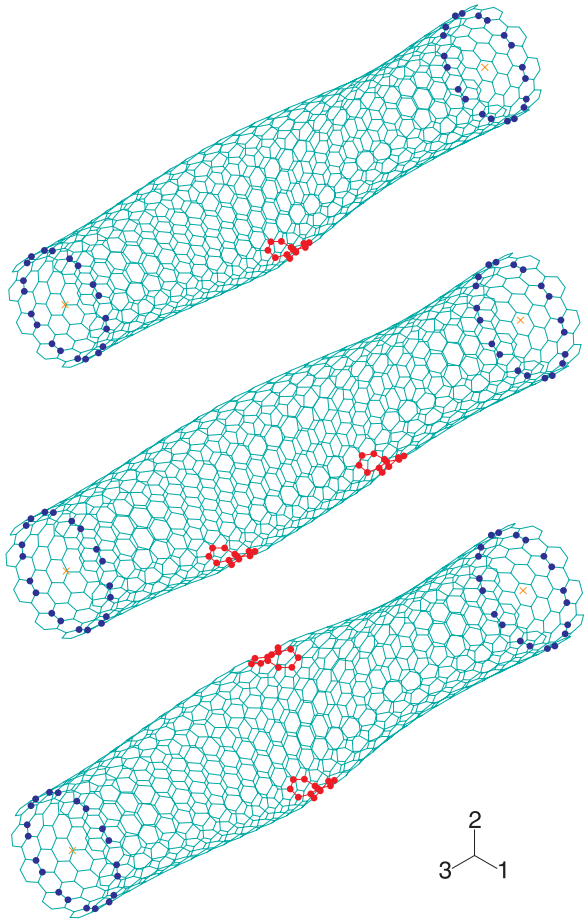

Figure 15 : Deformed configuration of the (10,10) armchair carbon nanotubes at torsion angle of about 40 degrees

4 Conclusions

Finite element simulations with a new four-node element based on the DREIDING potential for the atomic interactions have been performed to study the mechanical properties of single-walled carbon nanotubes with and without Stone-Wales defects under three main deformation modes: uniaxial tension, bending and torsion. The results obtained for geometrically perfect nanotubes of types (17,0) and (10,10) in the pre-failure states are in good agreement with those by Zhou and Shi (2001) based on molecular dynamics simulations using Brenner's potential. Nevertheless, the ultimate loads predicted by the two methods differ from each other. A reason for this is the difference between DREIDING potential and this of Brenner which becomes more important if the atomic distances are far from the equilibrium value. The post-failure response of the nanotube is governed by the breaking and the rearrangement of carbon bonds which can be simulated with the molecular dynamics approach based on Brenner's potential but not with the finite element method presented by the authors. The post-failure states of the nanotubes require special attention because in this case the atomic distances are so far from the equilibrium values that a force field method is eventually not adequate for their simulation.

Since the defects have a great effect on the ultimate loads of the nanotubes, we introduced a defect distribution function which specifies all defects in the nanotube by their lattice indices. For real-world simulations, this function should be formulated on the basis of experiments and an accompanying statistical investigation. Here, we restricted our calculations to systems with maximum two Stone-Wales defects equally distributed along the axis of the nanotube or in circumferential direction. We found that the influence of the defect distribution on the ultimate loads and moments depends significantly on both, the loading case and the number and location of the defects. While the ultimate load for the uniaxial tension case is almost the same for all defect distributions under consideration, the ultimate bending moment was influenced clearly by the number and the location of the Stone-Wales defects. An interesting behavior was observed for the defective (10,10) armchair carbon nanotube under torsion. In this case, the reduction of the ultimate moment due to the occurrence of initial Stone-Wales defects is with about 40 % very high but almost independent on the number and location of the defects. Of course, this result should not be generalized because it will be valid in this form only for the very restricted defect distributions discussed in this paper.

Acknowledgement: The authors gratefully acknowledge the stimulating discussions with Dr. Andreas Schneider, Institute for Inorganic Chemistry, University of Hannover.

References

Atluri, S. N. (2004): *The Meshless Method (MLPG) for Domain & BIE Discretizations*. Tech Science Press, Forsyth, GA.

Belytschko, T.; Xiao, S. P.; Ruoff, R. (2002): Effects of defects on the strength of nanotubes: Experimental-computational comparisons. arxiv.org e-Print archive, physics/0205090, 2002.

Brenner, D. W.; Shenderova, O. A.; Areshkin, D. A.; Schall, J. D.; Frankland, S.-J. V. (2002): Atomic modeling of carbon-based nanostructures as a tool for developing new materials and technologies. *CMES: Computer Modeling in Engineering & Sciences*, vol. 3, no. 5, pp. 643–674.

Buongiorno Nardelli, M.; Yakobson, B. I.; Bernholc, J. (1998): Brittle and ductile behavior in carbon nanotubes. *Physical Review Letters*, vol. 81, no. 21, pp. 4656–4659.

Buongiorno Nardelli, M.; Yakobson, B. I.; Bernholc, J. (1998): Mechanism of strain release in carbon nanotubes. *Physical Review B*, vol. 57, no. 8, pp. 4277–4280.

Chung, P. W.; Namburu, R. R.; Henz, B. J. (2003): A lattice statics-based tangent-stiffness finite element method. *CMES: Computer Modeling in Engineering & Sciences*, vol. 5, no. 1, pp. 45–62.

Crisfield, M. A. (1996): *Non-linear Finite Element Analysis of Solids and Structures – 1: Essentials*. John Wiley & Sons.

Crisfield, M. A. (1997): *Non-linear Finite Element Analysis of Solids and Structures – 2: Advanced Topics*. John Wiley & Sons.

Desch, C. (1934): *The Chemistry Of Solids*. Cornell University Press.

Dunlap, B. I.; Brenner, D. W.; Schriver, G. W. (1994): Symmetric isomers of hydrofullerene c60h36. *Journal of Physical Chemistry*, vol. 98, pp. 1756–1757.

Ghoniem, N. M.; Cho, K. (2002): The emerging role of multiscale modeling in nano- and micro-mechanics of materials. *CMES: Computer Modeling in Engineering & Sciences*, vol. 3, no. 2, pp. 147–173.

Mayo, S. L.; Olafson, B. D.; Goddard (III), W. A. (1990): DREIDING: A generic force field for molecular simulations. *Journal of Physical Chemistry*, vol. 94, pp. 8897–8909.

Miyamoto, Y.; Rubio, A.; Berber, S.; Yoon, M.; Tománek, D. (2004): Spectroscopic characterization of Stone-Wales defects in nanotubes. *Physical Review B*, vol. 69, pp. 121413/1–4.

Morse, P. M. (1929): Diatomic molecules according to the wave mechanics II: Vibrational levels. *Physical Review*, vol. 34, pp. 57–64.

Mowrey, R. C.; Brenner, D. W.; Dunlap, B. I.; Mintmire, J. W.; White, C. T. J. (1991): Simulations of buckminster fullerene (c60) collisions with a hydrogen-terminated diamond $\{111\}$ surface. *Journal of Physical Chemistry*, vol. 95, pp. 7138–7142.

Nasdala, L.; Ernst, G. (accepted): Development of a 4-node finite element for the computation of nano-structured materials. *Computational Materials Science*.

Saito, R.; Dresselhaus, G.; Dresselhaus, M. S. (1998): *Physical properties of carbon nanotubes*. Imperial College Press, London.

Shen, S.; Atluri, S. N. (2005): A tangent stiffness MLPG method for atom/continuum multiscale simulation. *CMES: Computer Modeling in Engineering & Sciences*, vol. 7, no. 1, pp. 49–68.

Srivastava, D.; Atluri, S. N. (2002): Computational nanotechnology: A current perspective. *CMES: Computer Modeling in Engineering & Sciences*, vol. 3, no. 5, pp. 531–538.

Srivastava, D.; Menon, M.; Cho, K. (2001): Computational nanotechnology with carbon nanotubes and fullerenes. *Computing in Science & Engineering*, vol. 3, no. 4, pp. 42–55.

Wei, C.; Cho, K.; Srivastava, D. (2003): Tensile strength of carbon nanotubes under realistic temperature and strain rate. *Physical Review B*, vol. 67, no. 11, pp. 115407/1–6.

Wei, C.; Srivastava, D.; Cho, K. (2002): Molecular dynamics study of temperature dependent plastic collapse of carbon nanotubes under axial compression. *CMES: Computer Modeling in Engineering & Sciences*, vol. 3, no. 2, pp. 255–262.

Yakobson, B. I.; Campbell, M. P.; Brabec, C. J.; Bernholc, J. (1997): High strain rate fracture and c-chain unraveling in carbon nanotubes. *Computational Materials Science*, vol. 8, no. 4, pp. 341–348.

Yang, L.; Han, J.; Anantram, M. P.; Jaffe, R. L. (2002): Bonding geometry and bandgap changes of carbon nanotubes under uniaxial and torsional strain. *CMES: Computer Modeling in Engineering & Sciences*, vol. 3, no. 5, pp. 675–686.

Yoon, M.; Han, S.; Kim, G.; Lee, S. B.; Berber, S.; Osawa, E.; Ihm, J.; Terrones, M.; Banhart, F.; Charlier, J.-C.; Grobert, N.; Terrones, H.; Ajayan, P. M.; Tománek, D. (2004): Zipper mechanism of nanotube fusion: Theory and experiment. *Physical Review Letters*, vol. 92, no. 7, pp. 075504/1–4.

Yu, M.-F.; Lourie, O.; Dyer, M. J.; Moloni, K.; Kelly, T. F.; Ruoff, R. S. (2000): Strength and breaking mechanism of multiwalled carbon nanotubes under tensile load. *Science*, vol. 287, no. 5453, pp. 637–640.

Zhang, P.; Lammert, P. E.; Crespi, V. H. (1998): Plastic deformations of carbon nanotubes. *Physical Review Letters*, vol. 81, no. 24, pp. 5346–5349.

Zhou, L. G.; Shi, S.-Q. (2001): Fracture strength of carbon nanotubes in hydrogen environment. In Tzeng, Y.; Miyoshi, K.; Yoshikawa, M.; Murakawa, M.; Koga, Y.; Kobashi, K.; Amaratunga, G. A. J.(Eds): *Proceedings of the Sixth Applied Diamond Conference/Second Frontier Carbon Technology Joint Conference*, pp. 773–778.